# Phase Stability of Garnet Solid-Electrolyte Interfacing with Various Cathodes in All Solid-State Batteries

To cite this article before publication: Chan-Yeop Yu *et al* 2022 *J. Electrochem. Soc.* in press https://doi.org/10.1149/1945-7111/ac4e5b

# Phase Stability of Garnet Solid-Electrolyte Interfacing with Various Cathodes in All Solid-State Batteries

| | |
|---|---|
| Journal: | *Journal of The Electrochemical Society* |
| Manuscript ID | JES-106474.R2 |
| Manuscript Type: | Research Paper |
| Date Submitted by the Author: | 01-Jan-2022 |
| Complete List of Authors: | Yu, Chan-Yeop; The Ohio State University<br>Choi, Junbin; The Ohio State University, Mechanical Engineering<br>Han, Jinhyup; Argonne National Laboratory<br>Lee, Eungje; Argonne National Laboratory,<br>Kim, Jung-Hyun; The Ohio State University, Mechanical and Aerospace Engineering |
| Keywords: | Solid-state lithium-ion battery, garnet-structured solid electrolyte, chemical stability, cathode-electrolyte interface, structural analysis |
| | |

# Phase Stability of Garnet Solid-Electrolyte Interfacing with Various Cathodes in All Solid-State Batteries

Chan-Yeop Yu,[1] Junbin Choi,[1] Jinhyup Han,[2] Eungje Lee,[2,z] and Jung-Hyun Kim[1,z]

[1]Mechanical and Aerospace Engineering, Center for Automotive Research, The Ohio State University, Columbus, Ohio 43210, United States

[2]Chemical Sciences and Engineering Division, Argonne National Laboratory, Lemont, Illnois, 60439 United States

[z]E-mail: kim.6776@osu.edu; eungje.lee@anl.gov

## Abstract

Garnet-structured $Li_{6.75}La_3Zr_{1.75}Ta_{0.25}O_{12}$ (LLZTO) is one of the most promising electrolyte materials for solid-state Li batteries (SS-LiB). The design and fabrication of a good cathode/electrolyte interface is an important criterion for the SS-LiB. In this work, we performed a systematic study on the impact of cathode crystal structure and chemical compositions on their chemical stabilities against the LLZTO at elevated temperatures, which are required for their adhesion during cell fabrication processes. X-ray Diffraction (XRD) and Rietveld refinement analyses revealed the chemical stabilities of various cathode materials in contact with the LLZTO. While layered $LiCoO_2$ cathode showed good stability in contact with LLZTO to 900 $^oC$, $LiNiO_2$ or Ni-rich $LiNi_xMn_yCo_{1-x-y}O_2$ (NMC) cathodes suffered from the formation of $La_4NiLiO_8$ due to La-diffusion from LLZTO. Mn-rich $LiMn_2O_4$ spinel and layered $LiNi_{1/3}Mn_{1/3}Co_{1/3}O_2$ cathodes suffered from the formation of $La_2Zr_2O_7$ due to Li-diffusion and production of $Li_2MnO_3$. As a result, $LiNi_{0.6}Mn_{0.2}Co_{0.2}O_2$, having an ideal balance of Ni/Mn/Co composition, or $Li_2MnO_3$ containing cathodes such as $Li_{1.2}Ni_{0.15}Mn_{0.55}Co_{0.1}O_2$ were found to having excellent phase stability as the cathodes for LLZTO-based SS-LiBs.


*This paper is part of the JES/JSS Joint Focus Issue In Honor of John Goodenough: A Centenarian Milestone*

## 1. Introduction

With the extensive growth of market demands for lithium-ion batteries (LiBs), enabling the large energy capacity for more powerful applications has been an important task for R&D. However, scaling up of LiBs brings about safety concerns. Conventional LiBs are intrinsically vulnerable to abusive conditions, such as internal/external short or poor thermal control. Due to flammable and volatile properties, organic liquid electrolytes in LiBs can act as a fuel for a thermal runaway.[1] To overcome such drawbacks of the conventional LiBs, solid-state Li batteries (SS-LiBs) have been

attracted as the next-generation energy storage device. Since SS-LiBs are not only fireproof but also enable to significantly increase the energy density, they have been under active investigations recently.[2,3]

Despite these advantages, the commercialization of SS-LiBs has been delayed by some technical challenges. One major challenge is related to interfaces between the electrode and solid electrolyte.[4–6] Unlike liquid – solid interface in conventional LiBs, good solid – solid interfaces in SS-LBs is difficult to achieve and maintain. A poor solid – solid contact impedes $Li^+$ transportation at the interface, resulting in increased cell impedance and subsequently impairing the cell operation. To obtain a good intergranular contact between the cathode and ceramic solid electrolytes such as $Li_7La_3Zr_2O_{12}$ (LLZO), they are sintered together at elevated temperatures (T > 500 $^oC$). However, sintering at such high temperatures can cause elemental interdiffusion and unwanted products at the cathode/electrolyte interfaces, which deteriorate Li-ion diffusion. For instance, it was observed that another type of solid electrolyte, $Li_{1.4}Al_{0.4}Ti_{1.6}(PO_4)_3$ (LATP) reacts with various cathode materials, producing secondary phases that limit the battery performances.[7] It was presented that the byproducts are likely to be insulators and thereby impede transportations of charge carriers during battery operations, which results in high resistance of the cells. Therefore, it is important to seek the optimum temperature and/or appropriate electrode/electrolyte materials combinations that can maintain a good cathode/electrolyte interface for manufacturing the solid-state devices.

Among the ceramic solid electrolyte, the garnet-structured $Li_{6.75}La_3Zr_{1.75}Ta_{0.25}O_{12}$ (LLZTO) has attracted some interests owing to its high Li-ionic conductivity of ~ $10^{-3}$ S/cm at 25 $^oC$, supported by its unique structure favorable to $Li^+$ conduction.[8,9]

There have been some reports regarding the chemical compatibility between garnet-type solid electrolyte and cathode materials. Kim et al.[10] prepared a thin-film interface of $LiCoO_2$ and LLZO and reported a formation of $La_2CoO_4$ phase after heating process. Ren et al.[11] screened the chemical compatibilities between LLZTO and different cathode materials including $LiCoO_2$, $LiMn_2O_4$, $LiNi_{0.33}Co_{0.33}Mn_{0.33}O_2$, and $LiFePO_4$. Although these literature offers good preliminary

data to explore the phase stabilities of cathodes in contact with the garnet solid electrolytes, it is timely to expand the scope of cathode materials aligned with the current R&D trend, which is moving forward to high-energy cathode materials such as Ni-rich $LiNi_xMn_yCo_{1-x-y}O_2$ (where $x \geq 0.6$) and Li-Mn-rich NMC (e.g., $xLi_2MnO_3 \cdot (1-x)LiMO_2$, where *M* refer to the transition metals).

In this context, the focus of this study is the impact of crystal structures and chemical compositions of the cathode materials on the stability against the LLZT. We designed and performed a comprehensive study by employing various cathode materials ($LiCoO_2$, $LiNiO_2$, NMCs, $LiMn_2O_4$, and $Li_{1.2}Mn_{0.55}Ni_{0.15}Co_{0.1}O_2$) and mixing them with LLZT at a specific ratio (e.g., 1:1 wt. ratio), which allows a lateral comparison for a series of the $LiNi_xMn_yCo_{1-x-y}O_2$ with a delicate compositional variation. A structural analysis using the Rietveld refinement was conducted to identify the reaction mechanism and quantify the byproducts.

## 2. Experimental

In this study, we used a commercial LLZTO solid electrolyte powder (Ampcera). $LiCoO_2$ (LCO) was synthesized by the simple solid-state method. Lithium hydroxide (Sigma-Aldrich) and cobalt hydroxide (Sigma-Aldrich) powders were mixed in stoichiometric amount and heated at 800 ℃ for 5 h. $LiNiO_2$ (LNO) was synthesized by the solid-state method. $LiOH \cdot H_2O$ and nickel hydroxide (Sigma-Aldrich) powders were mixed in 1.05:1 molar ratio and heated at 800 ℃ for 5 h. $LiMn_2O_4$ and $Li_2MnO_3$ were synthesized via a solid-state reaction method. $Li_2CO_3$ (Fisher chemical) and $Mn_2O_3$ (Alfa Aesar) were mixed with stoichiometric ratio, then heat-treated at 750 ºC for 20 h. $Li_{1.2}Ni_{0.15}Mn_{0.55}Co_{0.10}O_2$ (LMR-NMC) was prepared by a sol-gel method. The stoichiometric amount of Li, Ni, Mn, and Co acetates (Alfa Aesar) was dissolved in aqueous solution and stirred at 60 ºC until it formed a gel. The gel was heat-treated at 900 ºC for 20 h. Commercial $LiNi_{0.33}Mn_{0.33}Co_{0.33}O_2$ (NMC111), $LiNi_{0.6}Mn_{0.2}Co_{0.2}O_2$ (NMC622), $LiNi_{0.8}Mn_{0.1}Co_{0.1}O_2$ (NMC811), $LiNi_{0.94}Co_{0.6}O_2$ (NC) powders were used. These commercial cathode powders have particle sizes in a range of 5 – 10 µm, whilst the LLZTO has ~ 500 nm particle size.

High-temperature chemical stability between LLZTO and various cathode materials (e.g., LCO, LNO, NMC, LNMO, or LMR-NMC) were performed by grinding mixtures of LLZTO and cathode powders with 1:1 wt. ratio, followed by heating those powders at 700 – 900 ºC for 2 h in air. After the heat treatment, X-ray Diffraction (XRD) patterns of powder samples were obtained using Rigaku SmartLab XRD (Cu K$\alpha$ radiation). The crystal phases of each sample were further characterized by the Rietveld refinement analysis of XRD data using the GSAS-II software.[12] To quantify the Li/Ni cation mixing, Li and Ni elements were placed in both 3a/3b sites by applying a restriction to make their sum of occupancies to be 1.0 at both sites. The cation mixing was simulated at the last step of the refinements.[13]

The electrochemical property of the heat-treated LLZTO/cathode composite powders (1:1 wt. ratio) was evaluated in Li-metal half-cells. Cathodes were prepared using the NMC/LLZTO mixture (1:1 wt. ratio) samples as an active material, Super P (Timcal) as a conductive agent, and PVdF (Kynar 900) as a binder. These components were mixed in 85:7.5:7.5 wt ratio with N-methylpyrrolidone (NMP) and coated on aluminum foil, and only the weight of the active materials were considered to determine the specific capacity of the cells. 1M $LiPF_6$ ethylene carbonate (EC)/ethylmethyl carbonate (EMC) (1:1 vol. ratio) worked as an electrolyte while polypropylene (Celgard 2500) was employed as a separator and Li-metal was utilized as an anode. Coin cells were cycled at the current density of 17 mA/g in the voltage range from 3.0 to 4.3V at 25 ºC using the Arbin cycler.

## 3. Results and discussion

### *Phase stabilities of LLZTO against $LiCoO_2$ and $LiNiO_2$*

$LiCoO_2$ (LCO), one of the most successful commercial layered cathodes, was studied as a baseline. Figure 1 shows the XRD patterns of the $LiCoO_2$/LLZTO mixture at different heating temperatures. The original structure was maintained regardless of the heating temperatures, suggesting that the $LiCoO_2$ cathode material has good chemical stability against the LLZTO at 700 – 900 ºC for 2 h. This behavior agrees very well with literature.[11] Although Kim et al. reported a formation of

$La_2CoO_4$ secondary phase (~ 100 nm thickness) at $LiCoO_2$/LLZO thin-film interfaces, it was speculated that the secondary phase was produced during the thin-film fabrication processes.[10] This result confirms that $LiCoO_2$ would be a good cathode material for the LLZTO-based solid-state battery cells. However, in recent years, there have been enormous efforts to reduce and further eliminate the Co element in cathode materials due to its high price, limited specific capacity, and toxicity. Hence, the focus of our study is investigating the chemical stabilities of various cathodes in contact with LLZTO.

As an alternative, Ni-rich cathodes have been actively investigated and implemented for commercial Li-ion batteries. For example, current R&D strives to increase the Ni contents in $LiNi_{1-x-y}Mn_xCo_yO_2$ to achieve high specific capacity while improving the phase stability of the materials.[14–16] In this regard, it is important to understand the phase stability of the end member, $LiNiO_2$, in contact with the LLZTO. Figure 2 displays XRD patterns of $LiNiO_2$/LLZTO mixture after heating at 700 − 900 °C for 2 h. It also plotted XRD peak positions of the layered-type cathode (ICSD# 090753) and garnet-type solid electrolyte (ICSD# 066647) as references.[17] At 700 °C, there was no significant change in the XRD pattern, indicating that the $LiNiO_2$ cathode material is chemically stable with the LLZTO up to 700 °C. At 800 °C, peaks corresponding to $La_4NiLiO_8$, an ordered perovskite phase, were found at 24.7°, 31.7°, and 42.6° in 2θ.[18] Lattice parameters of the $La_4NiLiO_8$ are a = 3.759 Å and c = 12.844 Å, which is very similar to the reference (lattice parameter a = 3.755 Å and c = 12.827 Å)[18], suggesting that its chemical composition will be close to the stoichiometric $La_4NiLiO_8$. Peak intensity from the ordered-perovskite grows further with increasing temperature from 800 °C to 900 °C for 2 h. Based on the Rietveld refinement analysis, the fractions of $La_4LiNiO_8$ phase were determined to be 2.3 and 8.5 wt.%, respectively, for 800 °C and 900 °C heated samples. It was recently reported that the $La_4LiNiO_8$ delivered a reasonable electrical conductivity of $3.5 \times 10^{-3}$ S $cm^{-1}$ at 30 °C.[19] However, the production of $La_4NiLiO_8$ secondary phase from our composite cathodes is accompanied by a phase decomposition of both $LiNiO_2$ cathode and LLZTO solid electrolyte. This will adversely affect the performance of the cathodes; since LLZTO offers the good

ionic conductivity, suppressing the formation of $La_4NiLiO_8$ and fully utilizing the capacity of $LiNiO_2$ cathode will be preferred in terms of cell energy density.

In addition, it is noticeable that $I(003)/I(104)$ peak ratio in the $LiNiO_2$ phase was decreased at 800 - 900 °C, indicating possible off-stoichiometry and $Ni^{2+}/Li^+$ cation mixing in the layered phase ($Li_{1-x}Ni_{1+x}O_2$; x>0).[20,21] Obtaining an ideal $LiNiO_2$ requires a careful synthesis conditions including a pure $O_2$ atmosphere. We observed an increased $Ni^{2+}/Li^+$ cation mixing in the $LiNiO_2$ powder when the synthesis atmosphere was changed from $O_2$ to air, as showin in Fig. S1. For example, the $O_2$ synthesized $LiNiO_2$ has 4.85% cation mixing whilst the air synthesized one has ~ 10% cation mixing. Hence, it will be reasonable to assume that the cation mixing in the $LiNiO_2$ is in part caused by heating in air. This result suggests that $O_2$ atmosphere will be required for the $LiNiO_2$ – electrolyte adhesion process during the solid-state battery fabrication.

***Phase stability of LLZTO against $LiNi_{1-x-y}Mn_xCo_yO_2$***

As an effort to reduce Co-contents, various chemical compositions in the $LiNi_{1-x-y}Mn_xCo_yO_2$ series have been developed for Li-ion battery applications.[22] In this study, we examined $LiNi_{0.33}Mn_{0.33}Co_{0.33}O_2$ (NMC111), $LiNi_{0.6}Mn_{0.2}Co_{0.2}O_2$ (NMC622), $LiNi_{0.8}Mn_{0.1}Co_{0.1}O_2$ (NMC811), and $LiNi_{0.94}Co_{0.06}O_2$ (NC946) cathode materials to find their phase stabilities against the LLZTO after heating the cathode + LLZTO mixtures at 700 – 900 °C. Figure 3 compares their representative XRD patterns obtained after heating at 900 °C for 2 h in air.

Figure S2 shows the XRD patterns of the NC946 (i.e., $LiNi_{0.94}Co_{0.06}O_2$) + LLZTO mixtures which were collected after heating them at 700 – 900 °C for 2 h in air. The NC946 was stable against the LLZTO after heating at 800 °C for 2 h but had the $La_4NiLiO_8$ peaks at 900°C of which quantity was determined to be 4.7 wt.% using the Rietveld refinement. Also, the NC946 layered phase in the mixture suffers from the $Ni^{+2}/Li^+$ cation mixing as evidenced by a significant decrease in the $I(003)/I(104)$ peak ratio after heating at 800 °C or 900 °C for 2 h in air. More interestingly, (003) peak at around 18.7° and (101) peak at around 36.4° in the NC946 layered phase were almost

vanished after heating at 900 ºC for 12 h in air, as shown in Fig. 4, which, in turn, transform into a rock-salt phase (i.e., Li/Ni disordering). Such abrupt phase degradation of NC946 would be related to its intrinsic thermodynamic instability under the given temperature and atmosphere. From the results, it is recommended to attach NC946 cathodes on LLZTO electrolyte at T < 900 ºC for 2 h in $O_2$ atmosphere while fabricating a solid-state battery cell.

Figure S3 shows the XRD patterns of the NMC811 + LLZTO mixtures which were collected after heating them at 700 – 900 ºC for 2 h in air. Although the XRD data did not show any secondary phases from the 800 ºC sample, the $La_4NiLiO_8$ were found again after heating at 900 ºC for 2 h. From Rietveld analysis, the amount of the $La_4NiLiO_8$ was determined to be 1.7 wt.%. In addition, it is noticeable that *I*(003)/*I*(104) peak ratio in the NMC811 phase was decreased at 900 ºC, indicating a $Ni^{2+}/Li^{+}$ cation mixing in the layered phase. When the heating period at 900 ºC was extended to 12 h, the *I*(003)/*I*(104) peak ratio in the NMC811 phase was decreased further as shown in Fig. 4. This result indicates a continuous increase in the $Ni^{2+}/Li^{+}$ cation mixing from the NMC811. At the same time, the intensities of $La_4NiLiO_8$ peaks did not increase from the XRD data. Similar to the $LiNiO_2$, the *I*(003)/*I*(104) peak ratio in the NMC811 phase was decreased after heating at 900 ºC for 2 h in air, indicating an off-stoichiometry and $Ni^{2+}/Li^{+}$ cation mixing in the layered phase. When the heating period at 900 ºC was extended to 12 h in air, the *I*(003)/*I*(104) peak ratio in the NMC811 phase was decreased further as shown in Fig. 4. This result indicates a continuous increase in the structural degradationof the NMC811 phase. At the same time, the intensities of $La_4NiLiO_8$ peaks did not increase from the XRD data. Therefore, adhesion process of the $LiNiO_2$ – electrolyte will require heating at $O_2$ atmosphere during the cell fabricaiton.

Figure S4 shows the XRD patterns of the NMC622 + LLZTO mixtures which were collected after heating them at 700 – 900 ºC for 2 h in air. The samples did not have noticeable peaks corresponding to the $La_2Zr_2O_7$ or the $La_4NiLiO_8$ after heating at 800 – 900 ºC for 2 h. Rietveld refinement analysis of the 900 ºC heated sample showed the minimal presence (0.8 wt.%) of $La_4NiLiO_8$, while the 800 ºC heated sample did not contain any impurity phases. This result suggests

a promising phase stability of the NMC622 in contact with LLZTO.

For NMC111, Fig. S5 revealed the formation of $La_2Zr_2O_7$ secondary phase after heating at 700 – 900 °C for 2 h. Rietveld refinement analysis quantified the amount of the $La_2Zr_2O_7$ to be 1.0 wt% from the sample heated at 900 °C for 2 h, as shown in Fig. 3. Considering that the $La_2Zr_2O_7$ is produced when Li-loss happens to LLZTO, its presence indicates a possible Li migration from LLZTO to the NMC111. As a result, it is speculated that Li-rich layered compound such as $Li_2MnO_3{\cdot}Li(Ni,Mn,Co)O_2$ is produced although its XRD patterns cannot be found probably due to its small amount or lack of crystallinity due to the short heating period (2 h). This assumption is supported by a fact that the formation of $La_2Zr_2O_7$ was suppressed with decreasing Mn contents (e.g., $x \leq 0.2$) in $LiNi_{1-x-y}Mn_xCo_yO_2$, which will be discussed in the later section. Although 2 h heating-period will be practical for the cathode – electrolyte adhesion process during a cell fabrication, we heated the NMC111 + LLZTO mixture at 900 °C for 12 h to observe their phase transition behavior during extended period of heating. The resulting XRD pattern (see, Fig. 4) shows peaks belong to the $La_4NiLiO_8$ that are absent from the 2 h heated sample, while still having the $La_2Zr_2O_7$ secondary phase.

It is notable that the increase in Ni content beyond the NMC622 leads to an unwanted production of $La_4NiLiO_8$ phase from the cathode + LLZTO mixture when heated at 900 °C for 2 h in air (see, Fig. 3). Under the same heating conditions, the amount of $La_4NiLiO_8$ phases increases from 1.7 wt.% for NMC811 to 4.7 wt.% for NC946. According to our results, NMC622 showed the best phase stability against the LLZTO among the various NMC cathode materials.

Although the Rietveld refinement determined the amount of impurity phases, sole structural data would not be enough to understand their impacts on the electrochemical performances. For example, specific capacities of the $LiNi_{1-x-y}Mn_xCo_yO_2$ cathodes are very sensitive to their stoichiometry, which can be altered slightly by participating in any unwanted chemical reactions with LLZTO. Therefore, we assessed the residual capacities of the cathodes in the cathode + LLZTO mixture by using conventional Li-ion battery half-cells. Figure 5 compares the electrical

performance of cathode (NMC111, NMC622, or NC946) + LLZTO mixtures which were heated at 900 °C for 2 h in air. In the mixtures, NMC111, NMC622, and NC946, respectively, delivered 58.5, 144.4, and 107.2 mAh/g of specific discharge capacities at the first two cycles. It is notable that the NMC111 lost around 60 % of original capacity of 159 mAh/g[22] even though the amount of the $La_2Zr_2O_7$ phase was only 1.0 wt.%. Such a small amount of $La_2Zr_2O_7$ phase would not be responsible for the major capacity fading. Instead, it suggests that the degradation of LLZTO in contact with NMC111 may involve a change in chemical composition and/or stoichiometry of NMC111 while maintaining the layered structure. For example, other elemental diffusions will potentially occur at elevated temperatures, including Zr-doping on NMC. It was reported that 1.7% (in terms of stoichiometric amount) Zr doping on NMC111 led to a capacity fading from 169.5 mAh/g to 144.9 mAh/g, which corresponded to 14.5 % capacity fading.[23] This result suggests that a slight deviation of stoichiometric composition into unwanted direction (e.g., possible La, Zr, Ta doping) can lead to a significant performance degradation. Such complex elemental inter-diffusion behaviors between cathode and $Li_{1.4}Al_{0.4}Ti_{1.6}(PO_4)_3$ solid-electrolyte and its significant capacity fading mechanism was also presented by Yu et al.[7] The NMC622 + LLZTO delivered the highest capacity among the three electrodes as anticipated from its good phase stability. However, it still experienced a slight capacity fading from its original capacity of 175 mAh/g,[22] which can be explained by the small fraction of $La_4NiLiO_8$ and consequent deviation of the chemical composition from the ideal NMC622. Finally, the NC946 + LLZTO also significantly lost its original capacity of ~ 200 mAh/g after heating at 900 °C for 2 h in air, which can be explained by the large amount of $La_4NiLiO_8$ (4.7 wt.%) that significantly alters the composition of NC946 cathode and the cation mixing.

***Phase stability of LLZTO against Mn-rich spinel and layered cathodes***

In the earlier section, NMC111 having a 1/3 stoichiometric amount of Mn in transition metal sites suffered from the unwanted Li migration from LLZTO to the NMC111 as evidenced by the formation of $La_2Zr_2O_7$ and consequent capacity degradation. Such side reaction mostly disappeared

when the Mn content was lower than 0.2 (i.e., $x \leq 0.2$ in $LiNi_{1-x-y}Mn_xCo_yO_2$), suggesting that the root-cause of Li migration is to form $Li_2MnO_3$ phase which is thermodynamic stable in the intermediate temperature range of 700 – 900 °C in air. Therefore, we further examined the phase stability of LLZTO in contact with various Mn-rich cathode materials such as $LiMn_2O_4$, $Li_2MnO_3$, and $Li_{1.2}Ni_{0.15}Mn_{0.55}Co_{0.10}O_2$ (LMR-NMC).[24,25]

Figure 6 shows the structural changes of the $LiMn_2O_4$ + LLZTO mixture after heating at 700 – 900 °C for 2 h in air. At 700 °C, most of the peaks corresponding to the LLZTO were disappeared while peaks corresponding to the $Li_2MnO_3$ phase newly appeared at around 20.7° – 24.1° in 2θ (ICSD# 073370)[26]. Figure S6 clearly demonstrates the formation of $Li_2MnO_3$ phase after heating at 900 °C for 2 h in air. With increasing the heating temperature, crystallization of the $La_2Zr_2O_7$ (ICSD# 022229)[27] was accelerated and became a dominant phase at 900 °C. This result agrees very well with our assumption - Mn in cathode materials prefers to accept extra Li-ion and transform into the Li-rich $Li_2MnO_3$ phase, which is accompanied by a phase transformation of the garnet to the Li-deficient $La_2Zr_2O_7$ phase. The $La_2Zr_2O_7$ will impede Li-ion transport due to its a lack of Li-ion conductivity and negatively impact on the cell performances.

In our previous work, we systematically presented that Li-concentration disparity between $Li_{1.4}Al_{0.4}Ti_{1.6}(PO_4)_3$ (LATP) and oxide cathode materials (e.g., layered and spinel phases) is the root cause of phase degradation at their interfaces after heating at high temperatures.[7] Table 1 shows that $LiMn_2O_4$ spinel has a Li-concentration value of 24.34 mol/L, which is much lower than 40.96 mol/L for the LLZTO. Such a large disparity will motivate a Li-diffusion from the LLZTO to the spinel. At the same time, it should be noted that the NMC111 had a high Li-concentration of 49.51 mol/L than that of the LLZTO but still experienced the Li-diffusion from LLZTO to NMC111. This result suggests that thermodynamic stability governs the elemental diffusion when the concentration disparity is not very large.

Since the $Li_2MnO_3$ was the secondary phase produced between the LLZTO and the Mn-rich compositions such as NMC111 and $LiMn_2O_4$, we examined the phase stability of the $Li_2MnO_3$ itself

against the LLZTO. Figure 7 shows the XRD patterns of $Li_2MnO_3$ + LLZTO mixtures collected after heating them at 700 – 900 °C for 2 h in air. All the peaks corresponded to their reference data for LLZTO and $Li_2MnO_3$ (ICSD#073370) without any impurity phases such as the $La_2Zr_2O_7$. The result unarguably demonstrates the superior phase stability of $Li_2MnO_3$ in contact with the LLZTO. As shown in Table 1, the relatively high Li-concentration of $Li_2MnO_3$ (63.8 mol/L) would impede the Li-diffusion from the LLZTO. On the other hand, the $Li_2MnO_3$ has a limited capability as a cathode in Li-ion batteries in terms of electrochemical performances although it can continuously cycle after its characteristic high-voltage reaction at around 4.5 $V_{vs.Li}$.[28]

Therefore, as a next step, we investigated the phase stability of the $Li_{1.2}Ni_{0.15}Mn_{0.55}Co_{0.10}O_2$ (LMR-NMC); alternatively can be expressed as $(0.5)Li_2MnO_3$–$(0.5)LiNi_{0.375}Mn_{0.375}Co_{0.25}O_2$. This composition has an integrated 'layered–layered' structure and has been actively investigated as a high-energy cathode material.[25] Figure 8 shows the XRD patterns of the LMR-NMC + LLZTO mixture after heating at 700 – 900 °C for 2 h in air. The 800 °C and 900 °C heated samples showed all the peaks corresponding to the reference patterns without forming the $La_2Zr_2O_7$ phase. The good phase stability of the LMR-NMC in contact with the LLZTO under the given heating conditions can be explained by the excellent thermodynamic stability of $Li_2MnO_3$ and its high Li-concentration (e.g., 56.57 mol/L in Table 1). However, the 700 °C heated sample still had minor peaks corresponding to the $La_2Zr_2O_7$. To carefully examine the phase stability of LMR-NMC + LLZTO mixture at 700 °C, this 700 °C annealed sample was re-ground to improve the mixing between LMR-NMC and LLZTO, followed by re-annealing at 700 °C for 2 h in air. The resulting XRD pattern, shown in Fig. S7c, even demonstrated a significant growth of the $La_2Zr_2O_7$ phase. This result suggests that the production of $La_2Zr_2O_7$ secondary phase is thermodynamically favored in our testing conditions, which may be associated with forming various Li – Mn – O compounds following their phase diagrams at such intermediate temperature.

## 4. Conclusion

Based on our systematic observation, it is found that the stabilities of the cathode / LLZTO interfaces strongly depend on the crystal structures and chemical compositions. Figure 9 illustrates the schematic diagram of the results. In layered cathodes, $LiCoO_2$ showed good phase stability, but $LiNiO_2$ formed $La_4NiLiO_8$-type ordered perovskite due to the La-diffusion. In the NMC system, NMC111 showed an impurity phase $La_2Zr_2O_7$ due to its large portion of the Mn source. From NMC811, the $La_2Zr_2O_7$ phase was suppressed but a new impurity phase $La_4NiLiO_8$ was formed after heat-treatment, of which behavior is similar to the $LiNiO_2$. Also, Ni-rich cathodes (e.g., $LiNiO_2$, NC946, NMC811) experienced $Ni^{2+}/Li^+$ cation mixing after heating in air, suggesting that cathode – electrolyte adhesion process requires heating in $O_2$ atmosphere during the cell fabrication. Among NMC family, NMC622 showed the best chemical stability in contact with the LLZTO due to its good Ni/Mn/Co compositional balance. In $LiMn_2O_4$ spinel, its large Li-concentration disparity comparing with the LLZTO accelerated the Li-ion diffusion and led to a significant phase transformation from LLZTO to the $La_2Zr_2O_7$. Both $Li_2MnO_3$ and LMR-NMC demonstrated good phase stabilities against the LLZTO due to their intrinsic phase stabilities, which encourages their applications for cathodes in all-solid-state batteries. Our results revealed the importance of customized process design of cathode – electrolyte interfaces to obtain ideal performances from all-solid-state batteries.

**ACKNOWLEDGMENT**

Characterization of this work was supported in part by The Ohio State University Institute for Materials Research. The work by J. Han and E. Lee was supported by Royalty funding through Argonne National Laboratory. Argonne is a U.S. Department of Energy laboratory managed by UChicago Argonne, LLC, under contract number DE-ACO2-06CH11357.

## References


(1) Mikolajczak, C.; Kahn, M.; White, K.; Long, R. T. *Lithium-Ion Batteries Hazard and Use Assessment*; Springer Science & Business Media, 2012.

(2) Wang, C.; Gong, Y.; Liu, B.; Fu, K.; Yao, Y.; Hitz, E.; Li, Y.; Dai, J.; Xu, S.; Luo, W.; Wachsman, E. D.; Hu, L. Conformal, Nanoscale ZnO Surface Modification of Garnet-Based Solid-State Electrolyte for Lithium Metal Anodes. *Nano Lett.* **2017**, *17* (1), 565–571. https://doi.org/10.1021/acs.nanolett.6b04695.

(3) Fu, K. (Kelvin); Gong, Y.; Liu, B.; Zhu, Y.; Xu, S.; Yao, Y.; Luo, W.; Wang, C.; Lacey, S. D.; Dai, J.; Chen, Y.; Mo, Y.; Wachsman, E.; Hu, L. Toward Garnet Electrolyte–Based Li Metal Batteries: An Ultrathin, Highly Effective, Artificial Solid-State Electrolyte/Metallic Li Interface. *Science Advances* **2017**, *3* (4), e1601659. https://doi.org/10.1126/sciadv.1601659.

(4) Hara, M.; Nakano, H.; Dokko, K.; Okuda, S.; Kaeriyama, A.; Kanamura, K. Fabrication of All Solid-State Lithium-Ion Batteries with Three-Dimensionally Ordered Composite Electrode Consisting of Li0.35La0.55TiO3 and LiMn2O4. *Journal of Power Sources* **2009**, *189* (1), 485–489. https://doi.org/10.1016/j.jpowsour.2008.12.048.

(5) Delaizir, G.; Viallet, V.; Aboulaich, A.; Bouchet, R.; Tortet, L.; Seznec, V.; Morcrette, M.; Tarascon, J.-M.; Rozier, P.; Dollé, M. The Stone Age Revisited: Building a Monolithic Inorganic Lithium-Ion Battery. *Advanced Functional Materials* **2012**, *22* (10), 2140–2147. https://doi.org/10.1002/adfm.201102479.

(6) Wang, Y.; Zhong, W.-H. Development of Electrolytes towards Achieving Safe and High-Performance Energy-Storage Devices: A Review. *ChemElectroChem* **2015**, *2* (1), 22–36. https://doi.org/10.1002/celc.201402277.

(7) Yu, C.-Y.; Choi, J.; Anandan, V.; Kim, J.-H. High-Temperature Chemical Stability of $Li_{1.4}Al_{0.4}Ti_{1.6}(PO_4)_3$ Solid Electrolyte with Various Cathode Materials for Solid-State Batteries. *J. Phys. Chem. C* **2020**, *124* (28), 14963–14971. https://doi.org/10.1021/acs.jpcc.0c01698.

(8) Xie, H.; Li, C.; Kan, W. H.; Avdeev, M.; Zhu, C.; Zhao, Z.; Chu, X.; Mu, D.; Wu, F. Consolidating the Grain Boundary of the Garnet Electrolyte LLZTO with $Li_3BO_3$ for High-Performance $LiNi_{0.8}Co_{0.1}Mn_{0.1}O_2$ /$LiFePO_4$ Hybrid Solid Batteries. *J. Mater. Chem. A* **2019**, *7* (36), 20633–20639. https://doi.org/10.1039/C9TA03263K.

(9) Zhao, Z.; Wen, Z.; Liu, X.; Yang, H.; Chen, S.; Li, C.; Lv, H.; Wu, F.; Wu, B.; Mu, D. Tuning a Compatible Interface with LLZTO Integrated on Cathode Material for Improving NCM811/LLZTO Solid-State Battery. *Chemical Engineering Journal* **2021**, *405*, 127031. https://doi.org/10.1016/j.cej.2020.127031.

(10) Kim, K. H.; Iriyama, Y.; Yamamoto, K.; Kumazaki, S.; Asaka, T.; Tanabe, K.; Fisher, C. A. J.; Hirayama, T.; Murugan, R.; Ogumi, Z. Characterization of the Interface between LiCoO2 and Li7La3Zr2O12 in an All-Solid-State Rechargeable Lithium Battery. *Journal of Power Sources* **2011**, *196* (2), 764–767. https://doi.org/10.1016/j.jpowsour.2010.07.073.

(11) Ren, Y.; Liu, T.; Shen, Y.; Lin, Y.; Nan, C.-W. Chemical Compatibility between Garnet-like Solid State Electrolyte Li6.75La3Zr1.75Ta0.25O12 and Major Commercial Lithium Battery Cathode Materials. *Journal of Materiomics* **2016**, *2* (3), 256–264. https://doi.org/10.1016/j.jmat.2016.04.003.

(12) Toby, B. H.; Von Dreele, R. B. *GSAS-II* : The Genesis of a Modern Open-Source All Purpose Crystallography Software Package. *Journal of Applied Crystallography* **2013**, *46* (2), 544–549. https://doi.org/10.1107/S0021889813003531.

(13) Thackeray, M. M.; Picciotto, L. A. de; David, W. I. F.; Bruce, P. G.; Goodenough, J. B. Structural Refinement of Delithiated LiVO2 by Neutron Diffraction. *Journal of Solid State Chemistry* **1987**, *67*, 285–290.

(14) Sun, Y.-K.; Myung, S.-T.; Park, B.-C.; Prakash, J.; Belharouak, I.; Amine, K. High-Energy Cathode Material for Long-Life and Safe Lithium Batteries. *Nature Materials* **2009**, *8* (4),

320–324. https://doi.org/10.1038/nmat2418.
(15) Kim, M.-H.; Shin, H.-S.; Shin, D.; Sun, Y.-K. Synthesis and Electrochemical Properties of Li[Ni0.8Co0.1Mn0.1]O2 and Li[Ni0.8Co0.2]O2 via Co-Precipitation. *Journal of Power Sources* **2006**, *159* (2), 1328–1333. https://doi.org/10.1016/j.jpowsour.2005.11.083.
(16) Schipper, F.; Erickson, E. M.; Erk, C.; Shin, J.-Y.; Chesneau, F. F.; Aurbach, D. Review—Recent Advances and Remaining Challenges for Lithium Ion Battery Cathodes: I. Nickel-Rich, LiNi $_x$ Co $_y$ Mn $_z$ O $_2$. *Journal of The Electrochemical Society* **2017**, *164* (1), A6220–A6228. https://doi.org/10.1149/2.0351701jes.
(17) Parise, J. B.; Harlow, R. L.; Shannon, R. D.; Kwei, G. H.; Allik, T. H.; Armstrong, J. T. Crystal Structure and Electron Microprobe Analyses of a Lanthanum Lutetium Gallium Garnet. *Journal of Applied Physics* **1992**, *72* (6), 2152–2155. https://doi.org/10.1063/1.351604.
(18) Li, G.; Yang, J.; Fan, Y.; Tian, S.; Zheng, C. Phase Equilibria of the System La2O3–NiO–Li2O at 700, 800, and 900°C. *Journal of Solid State Chemistry* **1998**, *141* (2), 457–461. https://doi.org/10.1006/jssc.1998.7978.
(19) Yasmin, A.; Shehzad, M. A.; Wang, J.; He, X.; Ding, X.; Wang, S.; Wen, Z.; Chen, C. La4NiLiO8-Shielded Layered Cathode Materials for Emerging High-Performance Safe Batteries. *ACS Appl. Mater. Interfaces* **2020**, *12* (1), 826–835. https://doi.org/10.1021/acsami.9b18586.
(20) Rougier, A.; Gravereau, P.; Delmas, C. Optimization of the Composition of the Li1 − z Ni1 + z O 2 Electrode Materials: Structural, Magnetic, and Electrochemical Studies. *J. Electrochem. Soc.* **1996**, *143* (4), 1168–1175. https://doi.org/10.1149/1.1836614.
(21) Ohzuku, T.; Makimura, Y. Layered Lithium Insertion Material of LiNi 1/2 Mn 1/2 O 2: A Possible Alternative to LiCoO 2 for Advanced Lithium-Ion Batteries. *Chemistry Letters* **2001**, *30* (8), 744–745.
(22) Choi, J.; Dong, L.; Yu, C.-Y.; O'Meara, C.; Lee, E.; Kim, J.-H. Relationship of Chemical Composition and Moisture Sensitivity in LiNi *x* Mn *y* Co1− *X* − *Y* O2 for Lithium-Ion Batteries. *Journal of Electrochemical Energy Conversion and Storage* **2021**, *18* (4), 041009. https://doi.org/10.1115/1.4051208.
(23) Lin, B.; Wen, Z.; Gu, Z.; Xu, X. Preparation and Electrochemical Properties of Li[Ni1/3Co1/3Mn1−x/3Zrx/3]O2 Cathode Materials for Li-Ion Batteries. *Journal of Power Sources* **2007**, *174* (2), 544–547. https://doi.org/10.1016/j.jpowsour.2007.06.125.
(24) Song, B.; Liu, H.; Liu, Z.; Xiao, P.; Lai, M. O.; Lu, L. High Rate Capability Caused by Surface Cubic Spinels in Li-Rich Layer-Structured Cathodes for Li-Ion Batteries. *Scientific Reports* **2013**, *3*. https://doi.org/10.1038/srep03094.
(25) M. Thackeray, M.; R. Croy, J.; Lee, E.; Gutierrez, A.; He, M.; Sun Park, J.; T. Yonemoto, B.; R. Long, B.; D. Blauwkamp, J.; S. Johnson, C.; Shin, Y.; F. David, W. I. The Quest for Manganese-Rich Electrodes for Lithium Batteries: Strategic Design and Electrochemical Behavior. *Sustainable Energy & Fuels* **2018**, *2* (7), 1375–1397. https://doi.org/10.1039/C8SE00157J.
(26) Riou, A.; Lecerf, A.; Gerault, Y.; Cudennec, Y. Etude structurale de Li2MnO3. *Materials Research Bulletin* **1992**, *27* (3), 269–275. https://doi.org/10.1016/0025-5408(92)90055-5.
(27) Sleight, A. W. New Ternary Oxides of Mercury with the Pyrochlore Structure. *Inorg. Chem.* **1968**, *7* (9), 1704–1708. https://doi.org/10.1021/ic50067a003.
(28) Guerrini, N.; Jin, L.; Lozano, J. G.; Luo, K.; Sobkowiak, A.; Tsuruta, K.; Massel, F.; Duda, L.-C.; Roberts, M. R.; Bruce, P. G. Charging Mechanism of Li2MnO3. *Chem. Mater.* **2020**, *32* (9), 3733–3740. https://doi.org/10.1021/acs.chemmater.9b04459.

**Table 1.** Lithium concentration of various cathodes and LLZTO solid-electrolyte materials.

| Material | $LiMn_2O_4$ | $Li_2MnO_3$ | NMC111 | LMR-NMC | LLZTO |
|---|---|---|---|---|---|
| Li concentration (mol/L) | 24.34 | 63.80 | 49.51 | 56.57 | 40.96 |

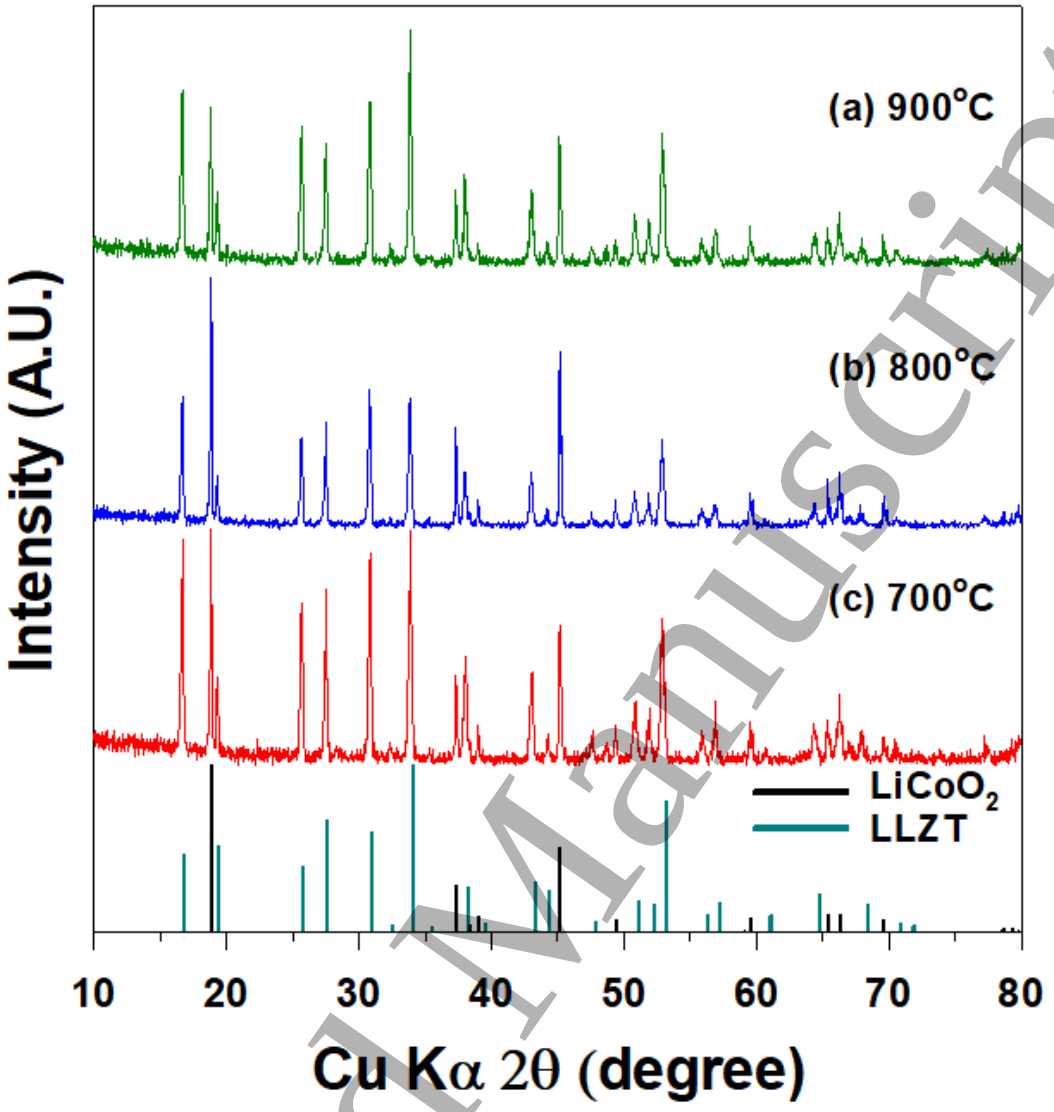


**Figure 1.** XRD patterns of the $LiCoO_2$-LLZTO mixture annealed at (a) 900°C, (b) 800°C, and (c) 700°C for 2 h in air, respectively.

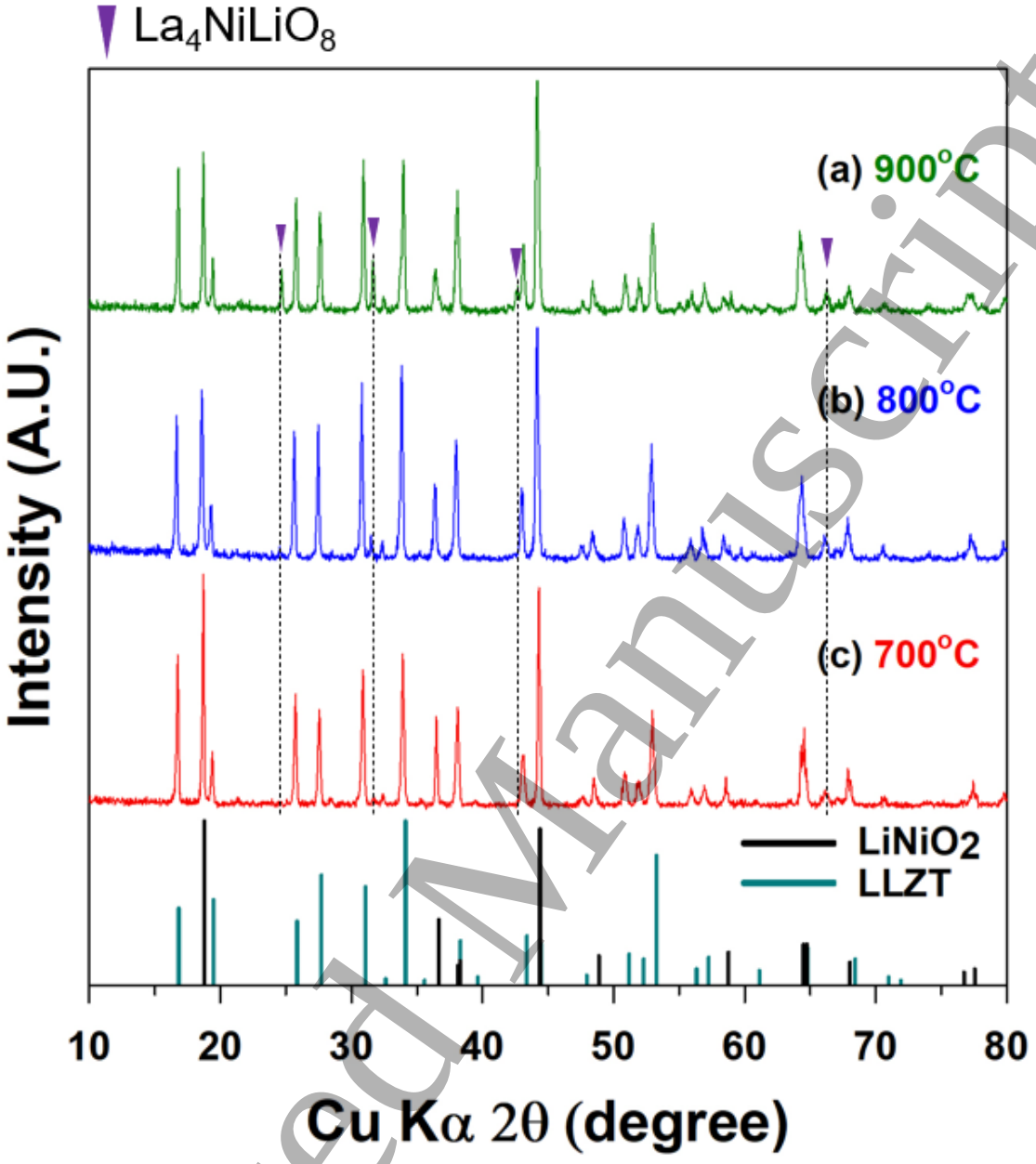


**Figure 2.** XRD patterns of the $LiNiO_2$-LLZTO mixture annealed at (a) 900°C, (b) 800°C, and (c) 700°C for 2 h in air, respectively. $La_4NiLiO_8$ phase was indexed by purple reversed triangle.

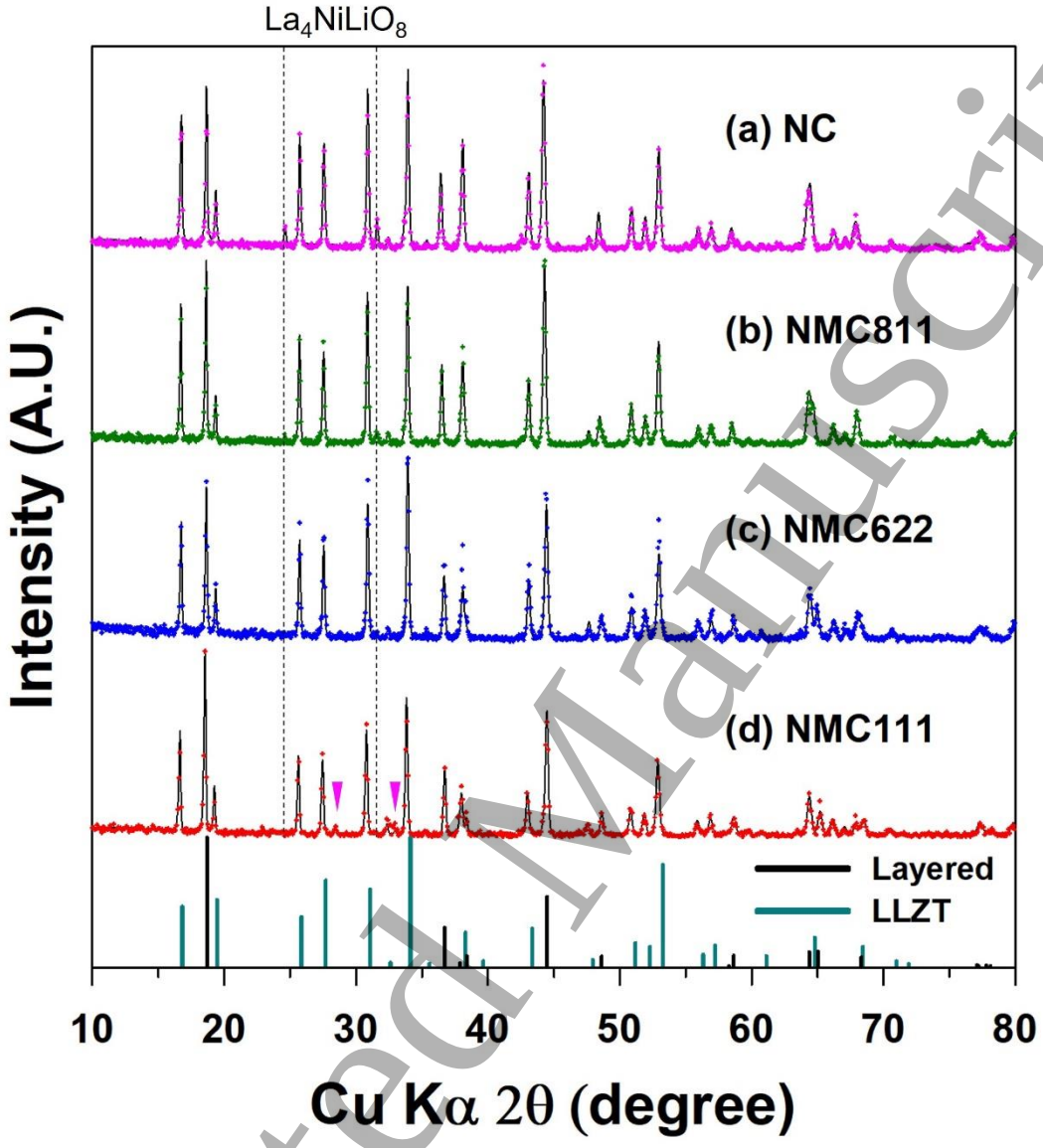


**Figure 3.** Rietveld refinement of the XRD patterns obtained from LLZTO + various NMC cathode materials mixtures annealed at 900 ºC for 2 h in air: (a) NC946, (b) NMC811, (c) NMC622, and (d) NMC111, respectively. Dots represent experimental data while solid represent simulated data. $La_4NiLiO_8$ peaks were indexed by dashed lines, and $La_2Zr_2O_7$ peaks were indexed by pink reversed triangles.

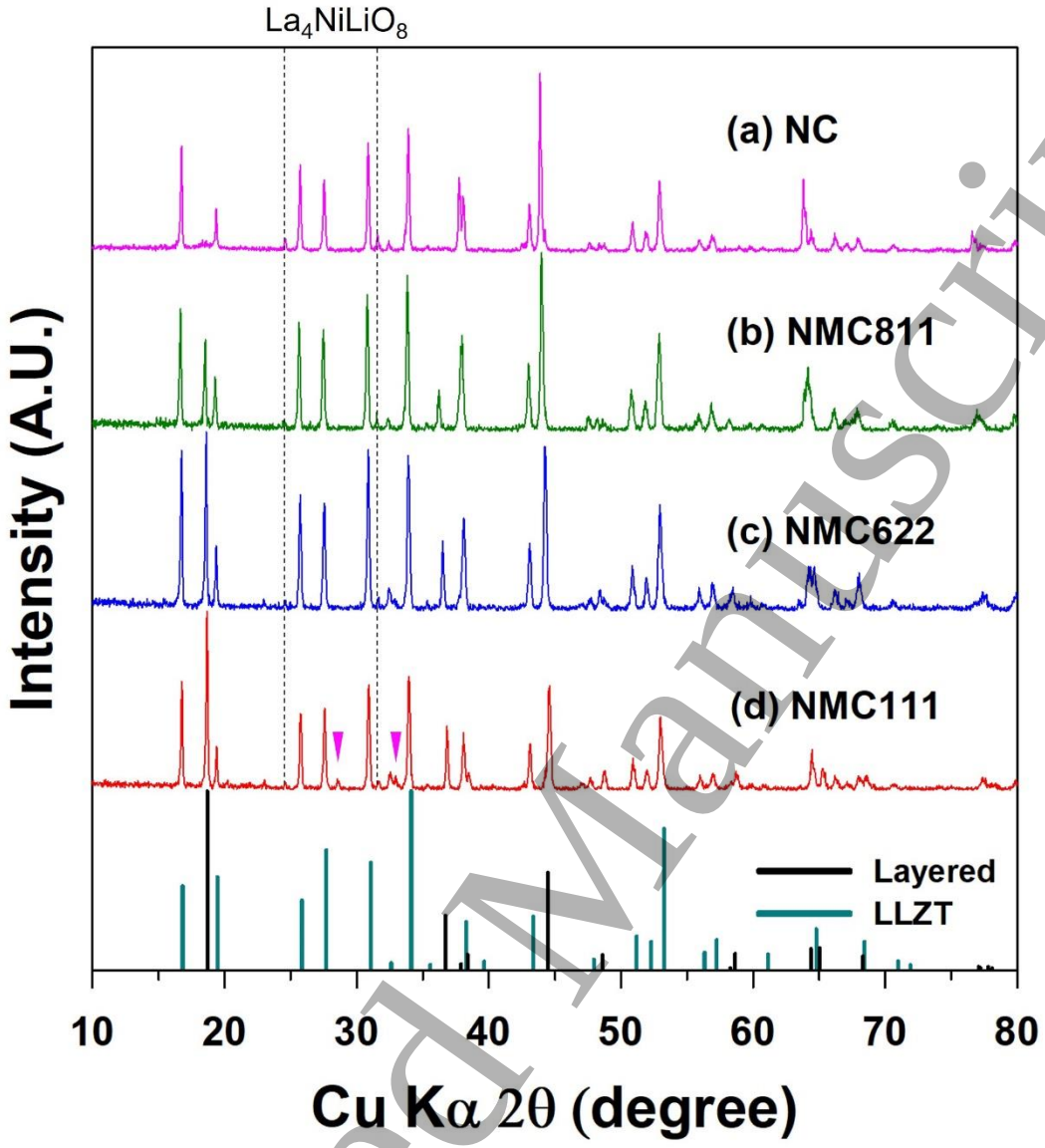


**Figure 4.** XRD patterns of the LLZTO – various NMC mixtures annealed at 900 ºC for 12 h in air. $La_4NiLiO_8$ peaks were indexed by dashed lines, and $La_2Zr_2O_7$ peaks were indexed by pink reversed triangles.

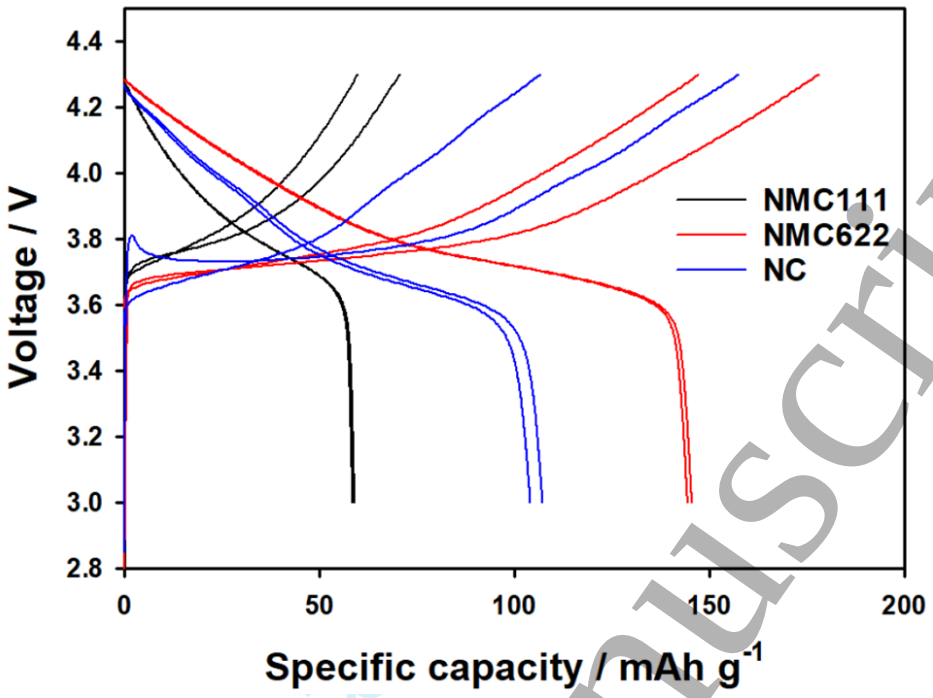


**Figure 5.** Electrochemical property of the LLZTO + various NMC mixed cathodes annealed at 900 $^{o}$C for 2 h in air at first two cycles. Conventional Li-ion half-cells were operated with 17 mA/g of current density in the voltage range from 3.0 to 4.3 $V_{vs.Li}$ at 25 $^{o}$C.

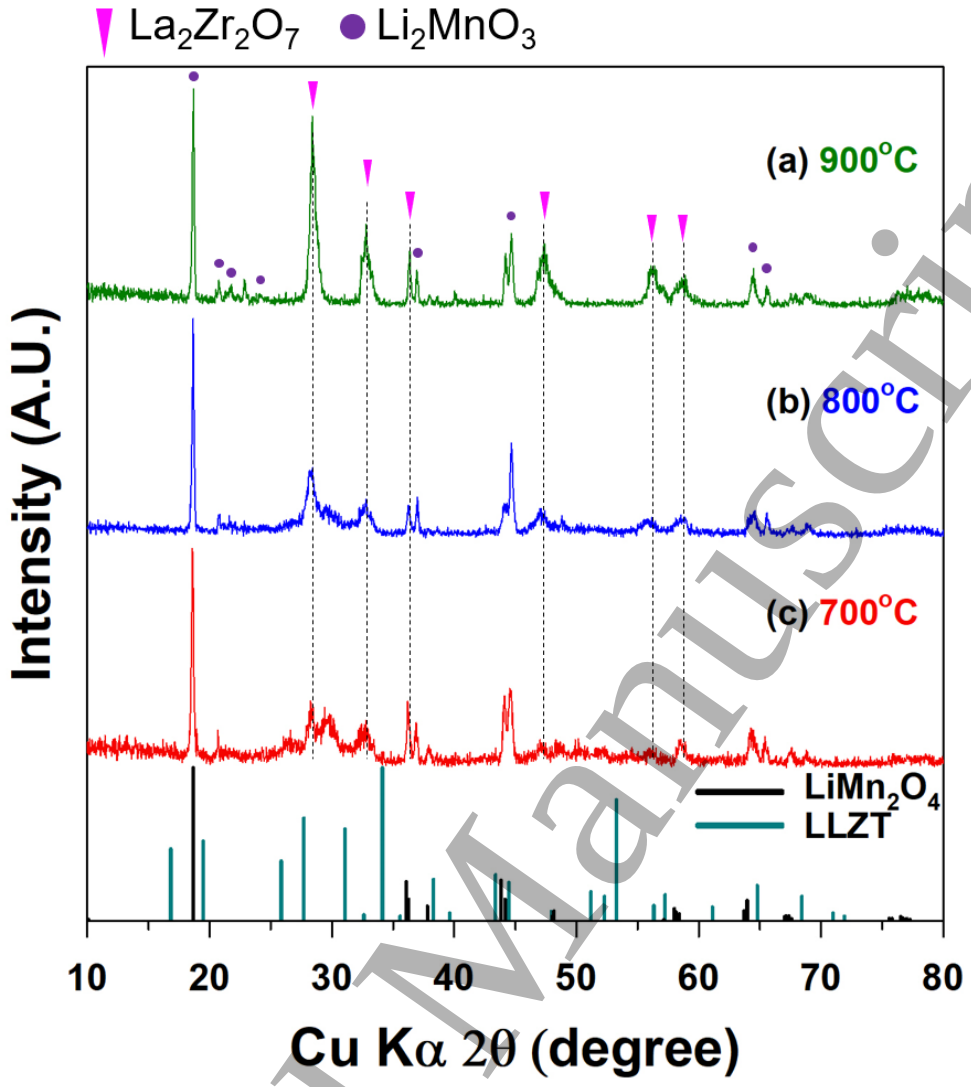


**Figure 6.** XRD patterns of the $LiMn_2O_4$-LLZTO mixture annealed at (a) 900ºC, (b) 800ºC, and (c) 700ºC for 2 h in air, respectively. The $La_4NiLiO_8$ phase was indexed by pink reversed triangle.

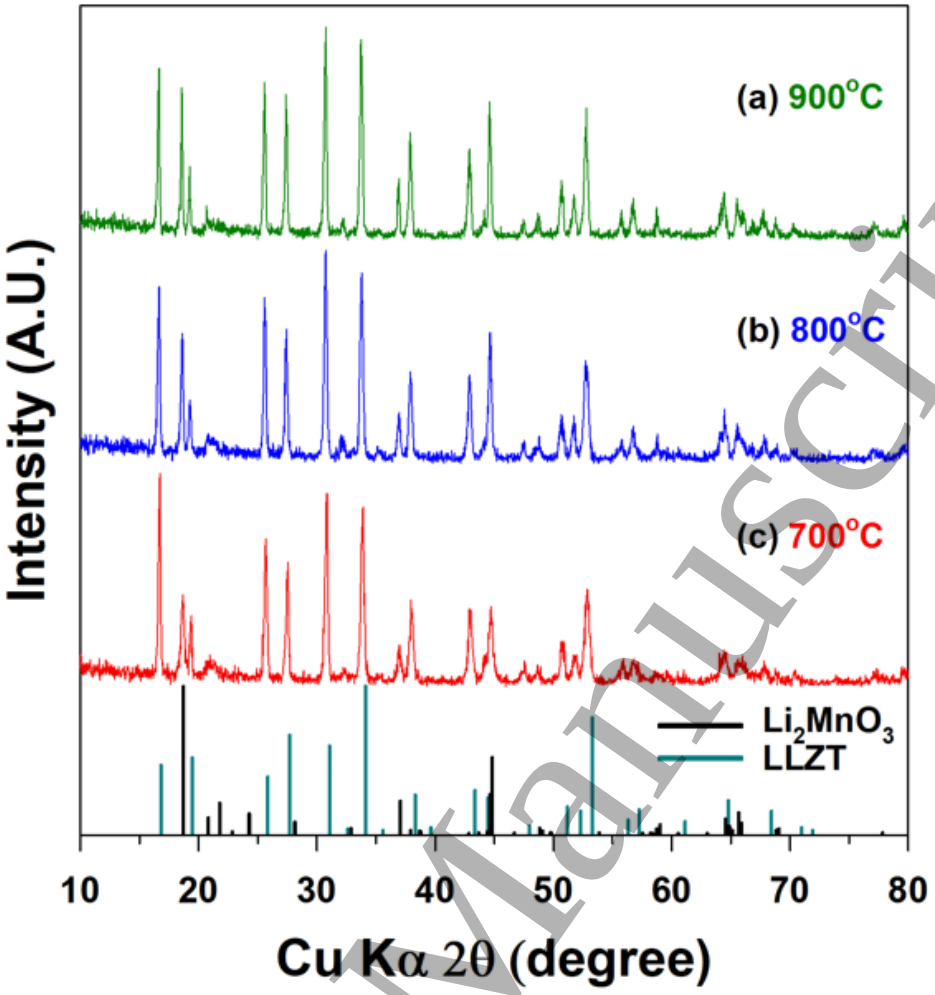


**Figure 7.** XRD patterns of the $Li_2MnO_3$-LLZTO mixture annealed at (a) 900°C, (b) 800°C, and (c) 700°C for 2 h in air, respectively.

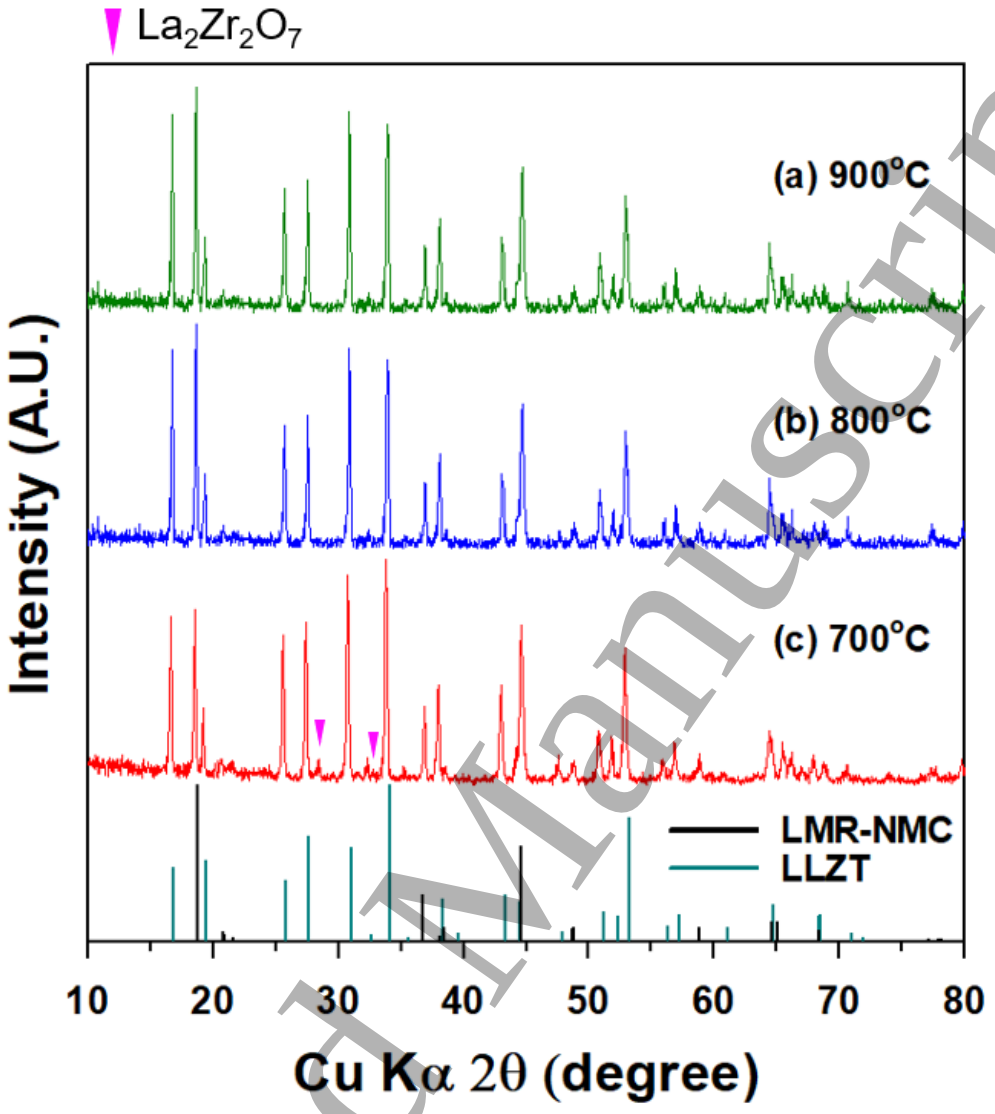


**Figure 8.** XRD patterns of the Li-Mn-rich NMC (LMR-NMC) − LLZTO mixture annealed at (a) 900°C, (b) 800°C, and (c) 700°C for 2 h in air, respectively.

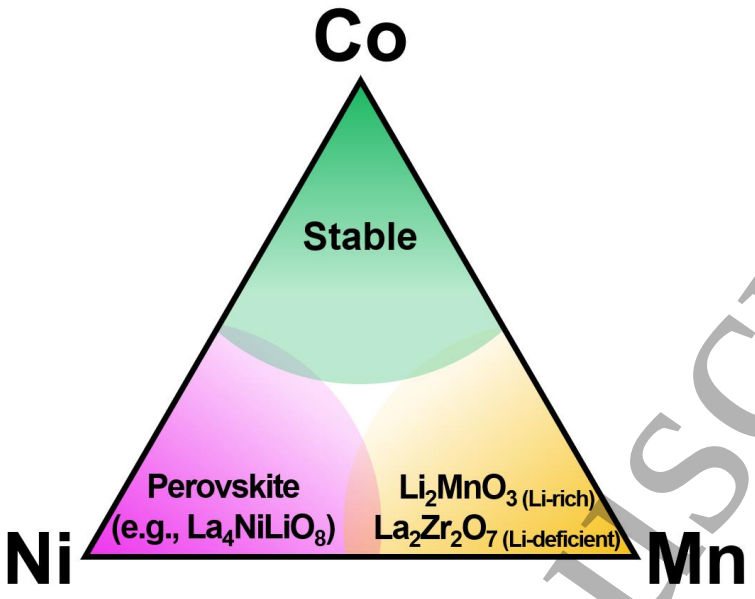


**Figure 9.** Schematic diagram illustrating the phase stability of LLZTO – cathode with various Ni/Co/Mn elements.